RSC Advances



PAPER

View Article Online

View Journal | View Issue



Cite this: RSC Adv., 2017, 7, 27024

Controlled synthesis of Sn-based oxides *via* a hydrothermal method and their visible light photocatalytic performances†

Jinghui Wang,^a Hui Li,^a Sugang Meng, ^b Xiangju Ye,*^b Xianliang Fu ^b*and Shifu Chen^{ab}

Controlled synthesis of Sn-based oxides with a different valence state is still a challenge. Here, we developed a facile hydrothermal method for selective preparation of SnO_2 , Sn^{2+} doped SnO_2 ($Sn^{2+} - SnO_2$), and SnO/SnO_2 composites, and SnO with $SnCl_2$ as a precursor. The valence state of Sn was regulated successively from Sn^{4+} to Sn^{2+} through controlling the hydrothermal solution from an O_2 -rich to an O_2 -deficient atmosphere, which was achieved by adding H_2O_2 or urea into the solution. The structure, absorption, morphology, and the visible light photocatalytic performance of the products were investigated systematically. SnO_2 , $Sn^{2+} - SnO_2$, SnO/SnO_2 , and SnO could be prepared in a H_2O_2 -contained, H_2O , urea-contained, and N_2 purged urea-contained solution, respectively. For $Sn^{2+} - SnO_2$, the doping amount of Sn^{2+} could be further tuned by varying the hydrothermal temperature, while for SnO/SnO_2 , the coupling amount of SnO could be controlled by the dosage of urea. Visible-light-induced photocatalytic degradation of methyl orange was achieved successfully on $Sn^{2+} - SnO_2$ and SnO/SnO_2 . However, further work is still required to improve the stability of the samples due to vulnerability of Sn^{2+} .

Received 9th April 2017 Accepted 16th May 2017

DOI: 10.1039/c7ra04041e

rsc.li/rsc-advances

1. Introduction

As a variable valence metal, Sn-based oxides can be in the form of univalent (SnO and SnO₂) or heterovalent oxides (Sn₂O₃ and Sn₃O₄, formed by regulating Sn²⁺/Sn⁴⁺ ratio¹). The univalent SnO and SnO₂ have attracted considerable attention during the past years because of their excellent optical, electrical, and electrochemical properties.2-8 For SnO, it can be used as anode materials in Li-batteries,7 coating materials,9 and catalysts for cyclization of maleamic acid.9 Furthermore, as Sn2+ can be easily oxidized to Sn⁴⁺ through a heat treatment in air, it can be used as a sacrificial template to prepare SnO2, another versatile Sn oxide. Due to its high optical transparency in the visible range, the remarkable receptivity to variation of gas, the low resistivity, and the excellent chemical stability, SnO2 has been extensively used in transparent conductive electrodes,4 gas sensors, 10,11 Li-batteries, 5 sensitized solar cells, 12 and photocatalysts. 13-15 To optimize the SnO and SnO2 performances,

various preparation methods including sol-gel, precipitation, hydrothermal, solvothermal, thermal evaporation, electrospinning, and laser ablation have been developed to manipulate their sizes, structures, and morphologes.8 Taking SnO2 as an example, the particle size can be reduced through a surfactantassisted solvothermal16 or hydrothermal77,18 route, while as for the morphologies, 0 to 3 dimensional SnO₂ nanostructures, such as nanoparticles, nanorods, nanowires, nanotube, nanosheets, and the 3D hierarchical architectures self-assembled from these low-dimensional nanostructures, have been subtly fabricated.8 Although the structure and the morphology of the Sn oxides can be readily controlled by using different preparation routes, there still is a lacks of a versatile fabrication route to control the component of the product, which is a key prerequisite for the applications. Most of the preparation methods are only suitable for the preparation of one of the Sn oxides.

Semiconductor-based photocatalytic technology possesses a great potential in the environmental remediation for its "green", high efficiency, and broad applicability. ^{19,20} Photocatalytic degradation of pollutants on Sn oxides, especially SnO₂, has been extensively investigated. Unfortunately, as a well-known n-type semiconductor, SnO₂ can only be activated under UV irradiation due to the wide-band gap energy (3.5–3.8 eV). ^{21–23} Furthermore, the activity is significantly restricted by the quick recombination of photo-induced charge carriers (e[–] and h⁺). Although the separation of e[–] and h⁺ can be improved by compositing SnO₂ with TiO₂, ^{24,25} ZnO^{26,27} and Zn₂SnO₄, ^{28,29} extending SnO₂ absorption to visible light range which accounts

^aCollege of Chemistry and Material Science, Huaibei Normal University, Huaibei, Anhui, 235000, China. E-mail: fuxiliang@gmail.com; Fax: +86-561-3090518; Tel: +86-561-3802235

^bDepartment of Chemistry, Anhui Science and Technology University, Fengyang, Anhui, 233100, China. E-mail: yexiangju555@126.com

[†] Electronic supplementary information (ESI) available: Degradation reaction system for MO, XPS spectrum of the prepared samples, time dependent UV-vis absorption spectrum of MO solution, chemical structure of MO, schematic band structures of the prepared samples, time dependent fluorescence spectra of the formed TAOH. See DOI: 10.1039/c7ra04041e

RSC Advances Paper

for 43% of the solar spectrum is still required to maximize the utilization of sunlight. Doping (non)-metallic elements is an effective strategy to narrow the band gap. However, the sample thermal stability and the separation of e⁻ and h⁺ are generally hampered by the doping with heterogeneous elements. These disadvantages can be avoided by a self-doping approach, 30-33 which introduces no impurity elements into the sample. The validity of the self-doping has been confirmed on the Ti³⁺ doped TiO₂ and some Sn²⁺ doped Sn ternary oxides (Sn²⁺-SnM₂O₆, M = Ta or Nb).34-36

Meanwhile, some other reports noted that SnO incorporated samples have a significant visible light activity in the degradation of organic pollutants. 1,37-40 These works arouse our interest that the visible light photocatalytic performance of SnO₂ may also can be promoted by doping with Sn²⁺ or incorporating with some Sn²⁺-contained species like SnO, Sn₂O₃ or Sn₃O₄. The visible light photocatalytic performances of some Sn²⁺-contained samples, such as SnO_{2-x}, 41 Sn₃O₄, 42 SnO-TiO₂, 43 SnO/ Sn₃O₄, and Sn₃O₄/TiO₂, demonstrate the feasibility of the strategy.

However, it remains difficult to incorporate Sn²⁺ species into SnO₂ as Sn²⁺ is easily oxidized to Sn⁴⁺. Controlling the Sn oxidation state is still a critical challenge. Recently, Fan's work41 indicates that Sn²⁺ self-doped SnO₂ can be skilfully prepared by a synproportionation reaction by adding Sn powder to the reaction solution: $Sn + Sn^{4+} \rightarrow Sn^{2+}$, while another work indicated that SnO and SnO2 can be selectively prepared by controlling the solution pH.45 These methods are limited to the preparation of one or two kinds of the Sn oxides. As far as we know, a facile method to synthesize a series of Sn oxides in a controlled way is still highly desired.

Herein, we developed a simple hydrothermal method to selective prepare a series of Sn oxides. Including SnO₂, Sn²⁺ doped SnO₂ (Sn²⁺-SnO₂), SnO/SnO₂ composite, and SnO were successfully synthesized through controlling the solution composition. The visible light photocatalytic performance of the samples was then evaluated by the degradation of methyl orange (MO) solution.

2. **Experiments**

Chemicals and preparation of Sn oxides

Analytical grade SnCl₂·2H₂O, urea (CO(NH₂)₂), H₂O₂, and MO were purchased from Aladdin Reagent Co. Ltd, Shanghai, China and used as received.

Preparation of Sn²⁺-SnO₂. 1 g SnCl₂·2H₂O was dissolved in 80 mL deionized water. After stirring for 30 min, the solution was then transferred into a Teflon-lined stainless autoclave and maintained at an elevated temperature for 24 h. The yellow products were centrifuged and rinsed alternatively in water and ethanol, and finally dried at 60 °C in a vacuum oven.

Preparation of SnO/SnO2. SnO/SnO2 was prepared via a similar hydrothermal process in urea-contained solution at 160 $^{\circ}$ C for 24 h.

Preparation of SnO and SnO₂. Pristine SnO₂ and SnO were synthesized in H₂O with 3 g urea added. For the preparation of SnO₂, 1 mL H₂O₂ (30%) was further added to promote the

conversion of Sn²⁺ to Sn⁴⁺ before the hydrothermal treatment at 160 °C, while for SnO, the solution was purged with N₂ before the treatment.

2.2 Characterization

X-ray diffraction patterns of the samples were recorded on a Brucker D8 Advance diffractometer. UV-visible diffuse reflection spectra (UV-vis DRS) were recorded on a Vis-NIR spectrophotometer (TU-1950, Persee) with BaSO₄ as a reference. Simultaneous thermal gravimetric analysis (TGA) and differential thermal analysis (DTA) of the Sn2+-SnO2 prepared at different temperatures were performed on a Shimadzu DTG-60H TG/DTA thermal analyser. N2 adsorption-desorption isotherms were obtained at 77 K by using a Micromeritics ASAP 2020 surface area analyzer. The morphologies were examined by a scanning electron microscopy (SEM, JSM-6610LV, Hitachi) and a transmission electron microscopy (TEM, FEI Tecnai G2 F20 S-TWIN). X-ray photoelectron spectroscopy (XPS) analysis was conducted on an ESCALAB 250 photoelectron spectrometer (Thermo Fisher Scientific) using Al Ka X-ray beam (1486.6 eV).

2.3 Photocatalytic decolorization of MO

Photocatalytic degradation of MO solution was carried out in a tubular reactor which was surrounded by a water cooling jacket. A 300 W Xe lamp (CEL-HXF300) was used as a light source with a UV cut off filter ($\lambda > 400$ nm). The picture of the reaction system can be found in Fig. S1 (see ESI†). In a typical experiment, 100 mg sample was dispersed in 100 mL 10 ppm MO. The suspension was then stirred for 30 min in the dark to reach an adsorption-desorption equilibrium. During irradiation, the solution temperature was controlled at 20 °C by a Julabo F12 cooling bath (Julabo Labortechnik, Germany). 3.8 mL suspension was withdrawn through a pipette every 10 min. The residual MO in the supernatant was monitored by a spectrophotometer (TU-1950, Persee).

2.4 Measurements of the photocurrent and the formation of hydroxyl radicals ('OH)

The photocurrent test was conducted on a CHI 660E electrochemical workstation (Chenhua, Shanghai) in a conventional three-electrode cell with Pt wire as the counter electrode, Ag/ AgCl electrode as the reference electrode, and the samples as the working electrode. The working electrode was fabricated by drop casting the sample powder dispersed water onto a FTO glass substrate (0.6 \times 0.6 cm) followed by drying the electrode at room temperature. 0.2 M Na₂SO₄ aqueous solution was used as the electrolyte.

The formations of 'OH in the photocatalytic process were determined by photoluminescence (PL) technique with terephthalic acid (TA) as a probe molecule. The procedure was similar to the degradation of MO except that the solution was replaced by 100 mL 5 imes 10⁻⁴ M TA and 2 imes 10⁻³ M NaOH mixed solution. The fluorescence signal of TAOH adduct was measured by a fluorescence spectrophotometer (JASCO FP-6500).

RSC Advances Paper

3. Results and discussion

3.1 Characterization of Sn²⁺-SnO₂ and SnO₂

Fig. 1a shows the XRD patterns of $\mathrm{Sn^{2+}}\text{-}\mathrm{SnO_2}$ prepared at different hydrothermal temperature. The diffraction peaks can be assigned to tetragonal $\mathrm{SnO_2}$ (JCPDS No. 77-447). The broad peaks at 2θ ca. 27, 34, and 52° can be ascribed to the reflections of the (110), (101), and (211) planes of $\mathrm{SnO_2}$. ⁴⁶ The intensity of these peaks improves gradually with the hydrothermal temperature, indicating that the crystallization of $\mathrm{SnO_2}$ is favoured by an elevated temperature. The top of Fig. 1a shows the XRD pattern of the prepared $\mathrm{SnO_2}$. The diffraction peak can be assigned to tetragonal $\mathrm{SnO_2}$ and are more pronounced and sharpened than the sample prepared in pure $\mathrm{H_2O}$. This result suggests that, besides the conversion of $\mathrm{Sn^{2+}}$ to $\mathrm{Sn^{4+}}$, the crystallization of $\mathrm{SnO_2}$ was also promoted by the addition of $\mathrm{H_2O_2}$. Similar function of $\mathrm{H_2O_2}$ has been reported. ^{47,48}

Fig. 1b shows the UV-vis DRS spectra of the Sn^{2+} – SnO_2 . An absorption threshold at *ca.* 500 nm can be observed and the absorption edge shows a blue-shift with the hydrothermal temperature. A change of the samples color from pale yellow to slight brown then can be observed (see the inset of Fig. 1b).

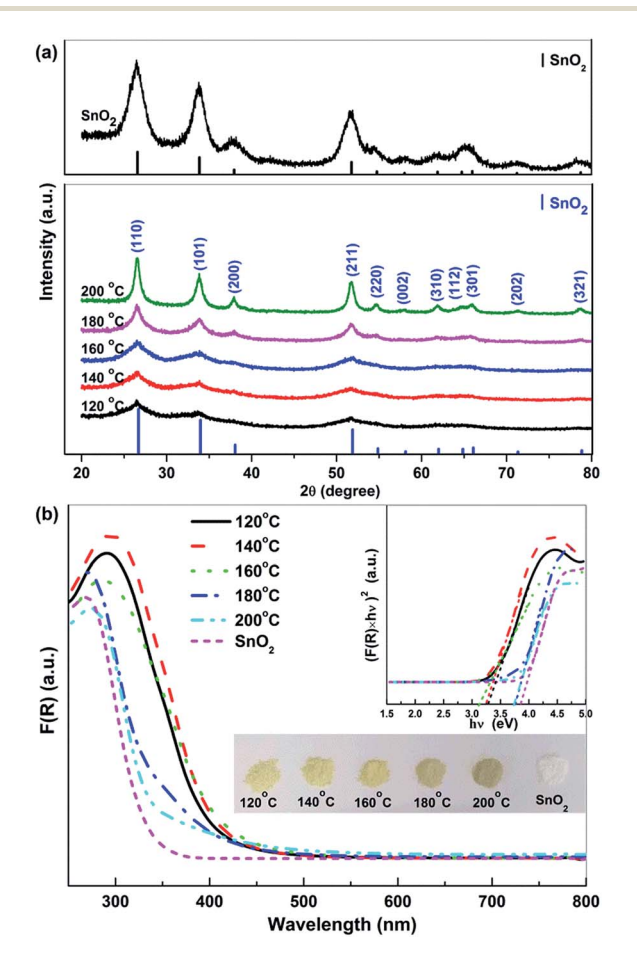


Fig. 1 (a) X-ray diffraction patterns and (b) UV-vis DRS spectra of the $\rm Sn^{2+}{-}SnO_2$ prepared at different temperatures and $\rm SnO_2$. The inset of (b) shows the corresponding Tauc plots and the appearance of the samples.

Although the samples show the same tetragonal structure as that of pristine SnO_2 , their colour is quite darker than SnO_2 , indicating the doping of Sn^{2^+} . As shown in the inset of Fig. 1b, Tauc plot approach⁴⁹ was used to determine Sn^{2^+} – SnO_2 band gap energy (E_g). The results (summarized in Table 1) indicate that, for the samples prepared below 160 °C, the E_g is only *ca.* 3.10 eV. Further enhancing the hydrothermal temperature to 200 °C, the samples E_g are close to 3.60 eV. The E_g of the prepared SnO_2 is 3.73 eV and it is consistent well with the reported value. Also solve of SnO could be extended to the visible light region by doping with Sn^{2^+} . This result clearly indicates that the absorption of SnO_2 could be extended to the visible light region by doping with Sn^{2^+} . As Sn^{2^+} tends to be oxidized to Sn^{4^+} at an elevated temperature, the increase of E_g with hydrothermal temperature should be caused by the reduction of Sn^{2^+} doping content.

 $SnO_2 \cdot H_2O$ shows a similar diffraction pattern to the tetragonal SnO_2 . TGA and DTA analyses of the prepared Sn^{2+} – SnO_2 were carried out to further corroborate the identification. As shown in Fig. 2a, an initial mass loss of 1.0% can be observed below 120 °C. It can be attributed to the dehydration of the adsorbed water, which leads to the endothermic peak in Fig. 2b. A second mass loss ca. 1.0% is occurred around 400 °C due to the volatilization of the contaminated Cl^- . After that, the TGA curves have no change. The result rules out the possibility that the products are $SnO_2 \cdot H_2O$ as its theoretical weight loss is larger than 10%. It also rules out the presence of SnO component in the samples, which shows a weight increases around $570 \, ^{\circ}C^{54}$ due to the oxidation of Sn^{2+} to Sn^{4+} . Thus, based on the results shown in Fig. 1 and 2, it can be deduced that the samples prepared at different temperatures in H_2O are Sn^{2+} – SnO_2 .

Fig. 3 shows the SEM images of the prepared $\mathrm{Sn^{2^+}\text{-}SnO_2}$. The samples prepared below 200 °C (Fig. 3a–d) are mainly composed of rods with a length of about 15 μ m and a diameter of about 3 μ m. With enhancing the preparation temperature, the surface of the rods becomes coarse and some small particles are present, suggesting the decomposition of the rods. When the temperature reaches 200 °C, no any rods can be observed (Fig. 3e). Pristine $\mathrm{SnO_2}$ prepared in the $\mathrm{H_2O_2\text{-}contained}$ solution (Fig. 3f) shows a similar morphology feature as the sample prepared at 200 °C.

3.2 Characterization of SnO/SnO₂ and SnO

Fig. 4a shows the XRD patterns of the SnO/SnO₂ prepared in different urea-contained solutions. When no urea was added, the resulted sample was Sn²⁺-SnO₂ as shown by Fig. 1. For the samples prepared in urea-contained solution, two sets of diffraction peaks originated from tetragonal SnO₂ (JCPDS No. 77-447) and SnO (JCPDS No. 78-1913) can be observed, confirming the formation of SnO/SnO₂ composite. As shown in the top of Fig. 4a, the diffraction pattern of the sample prepared in N₂ purged solution can be assigned to SnO, along with two very small diffraction peaks of SnO₂ (110) and (211).

Fig. 4b shows the UV-vis DRS of the prepared $SnO-SnO_2$ and SnO. The composite show an apparent visible light absorption and the thresholds extend to ca. 700 nm. With an increase of urea dosage, the absorption coefficient of the resulted SnO-

Table 1 Summary of the hydrothermal conditions and the characterization results of the $E_{\rm g}$ and the BET surface area of the prepared Sn oxides

| Reaction condition | | Product | $E_{ m g}$ (eV) | BET area (m ² g ⁻¹) |
|--|-----|---|-----------------|--|
| Temp. (°C) (without urea) | 120 | Sn ²⁺ -SnO ₂ | 3.20 | 100.1 |
| | 140 | | 3.13 | _ |
| | 160 | | 3.10 | 116.4 |
| | 180 | | 3.59 | _ |
| | 200 | | 3.60 | 99.9 |
| Urea (g) (temp. 160 $^{\circ}$ C) | 0 | $\mathrm{Sn}^{2+}	ext{-}\mathrm{SnO}_2$ | 3.14 | 116.4 |
| | 0.5 | SnO/SnO_2 | 3.41 | _ |
| | 1.0 | | 3.34 | 79.2 |
| | 2.0 | | 3.04 | _ |
| | 3.0 | | 3.08 | 77.1 |
| 3 g urea + 1 mL H_2O_2 , 160 °C | | SnO_2 | 3.73 | 173.3 |
| 3 g urea + N ₂ purged, 160 °C | | SnO | 2.71 | 5.2 |

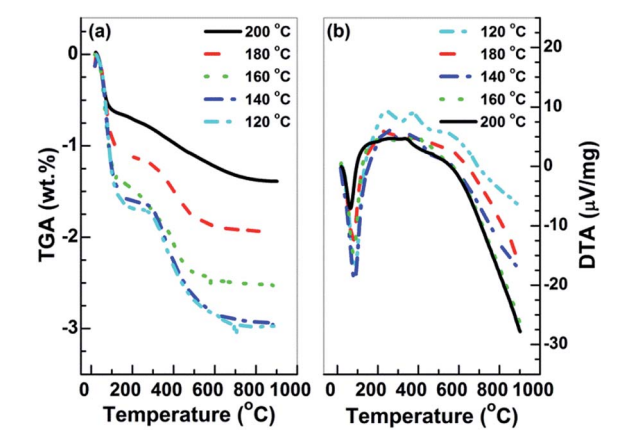


Fig. 2 (a) TGA and (b) DTA curves of the ${\rm SnO_2}$ prepared at different temperatures.

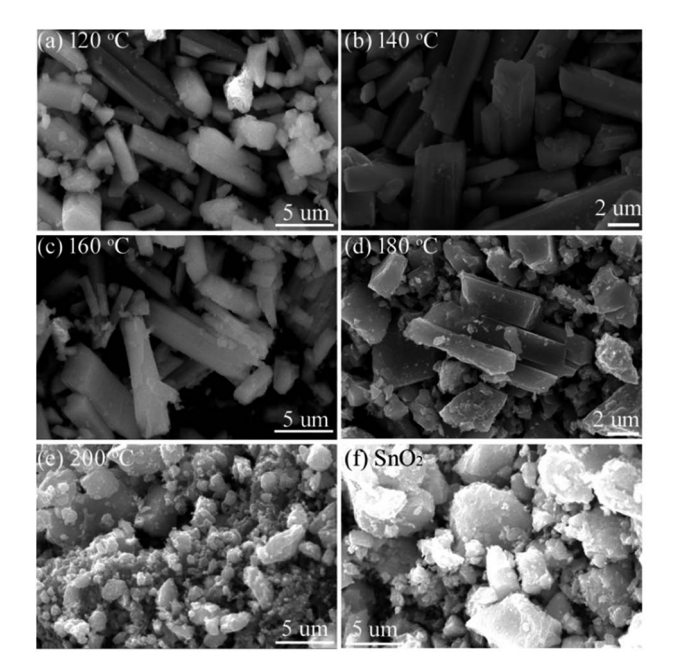


Fig. 3 SEM images of the samples prepared at different temperatures (a) 120, (b) 140, (c) 160, (d) 180, (e) 200 °C, and (f) SnO $_2$ prepared at 160 °C in $\rm H_2O_2$ -contained solution.

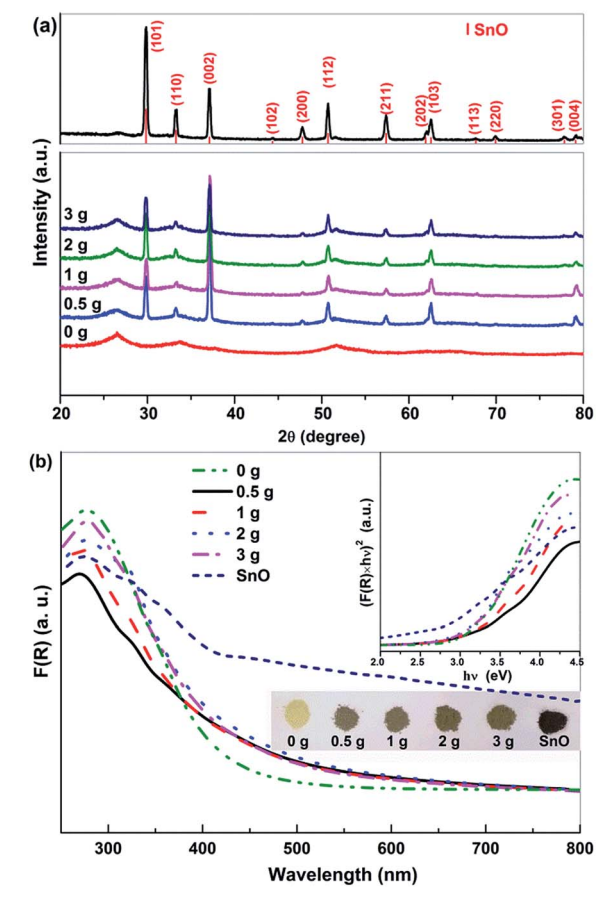


Fig. 4 (a) X-ray diffraction patterns and (b) UV-vis DRS spectra of the SnO/SnO_2 composites prepared in different urea-containing solutions and the prepared SnO. The inset shows the corresponding Tauc plots and the appearance of the samples.

 ${\rm SnO_2}$ is improved and the sample colour changes from slight brown to dark brown as shown in the inset of Fig. 4b. The absorption of ${\rm SnO/SnO_2}$ is gradually extended to the visible range with an increase of urea dosage. SnO shows the highest visible light absorption coefficient due to its black colour and the $E_{\rm g}$ is 2.71 eV, agreeing well with the reported result. The $E_{\rm g}$

RSC Advances Paper

of SnO/SnO₂ samples were estimated by Tauc plots (the inset of Fig. 4b) and the results are summarized in Table 1.

Fig. 5 shows the SEM images of the prepared SnO/SnO_2 . Resembling the sample prepared in water (without urea, Fig. 5a), rod-like samples (Fig. 5b–e) with a length of about 15 μ m and a diameter of about 3 μ m were also obtained in the urea-contained solution. However, a decomposition of the rods can be observed with an increase of urea dosage and the surface becomes rough (Fig. 5b–e). Some small particles then appear and distribute on the rods surface. As shown in Fig. 5f, the morphology of the prepared SnO is quite different to SnO/SnO_2 composites. The sample is composed of many tightly aggregated strips.

The morphology feature of the SnO/SnO2 was further characterized by TEM using the sample prepared in 3 g ureacontained solution as a representative. As shown in Fig. 6a and b, some nanosheets and small rods with a diameter of ca. 10 nm and a length of ca. 300 nm (indicated by the arrows in Fig. 6b) can be observed. The small rods are covered by the nanosheets. The SAED pattern in Fig. 6c indicates the polycrystalline nature of the nanosheets. The diffraction rings from the inner to outward can be indexed to the (110), (101), (200), and (211) planes of SnO₂, respectively. Two sets of lattice space with d values of 0.26 and 0.33 nm can be found in the HRTEM images (Fig. 6d and e), which corresponds to the (101) and (110) planes of tetragonal SnO2. The results suggest that the sheetlike particles are SnO₂. As for the small rods, the HRTEM image (Fig. 6f) demonstrates that the d value of the lattice space is 0.29 nm, which corresponds to the (101) plane of SnO. 43 Thus, the small rods are SnO. Similar structure of SnO has been reported in SnO/SnO₂ composite.⁴⁰

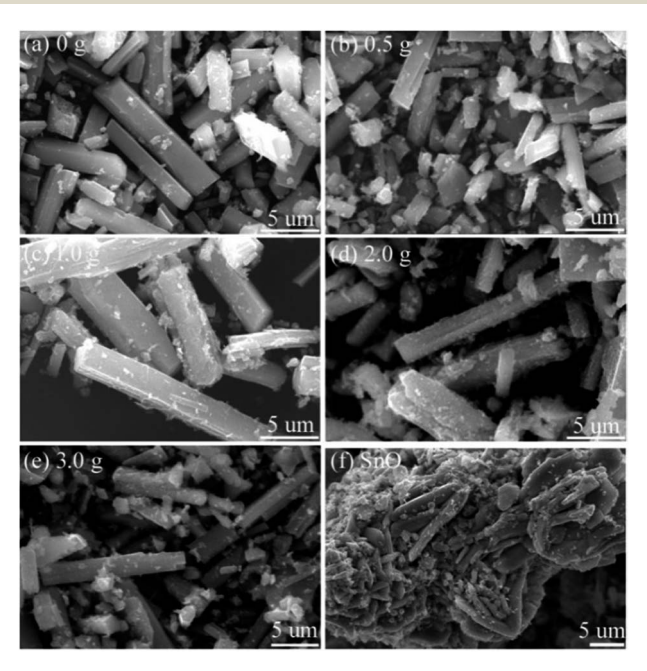


Fig. 5 SEM images of the samples prepared in different urea-contained solutions (a) 0, (b) 0.5, (c) 1.0, (d) 2.0, (e) 3.0 g, and (f) the prepared SnO.

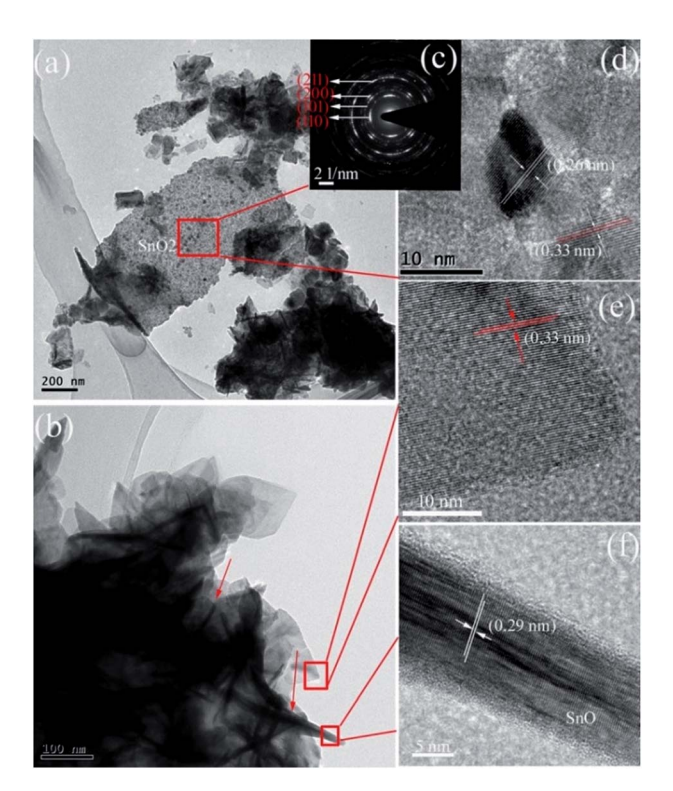


Fig. 6 (a and b) TEM, (c) SAED, and (d-f) HRTEM images of the prepared $SnO-SnO_2$ in 3 g urea-contained solution.

Some of the prepared samples including SnO_2 , Sn^{2+} – SnO_2 , SnO/SnO_2 and SnO were analyzed by XPS to study the chemical states of Sn and O. The survey spectra (Fig. S2-a†) clearly indicate that, besides the adventitious C, the samples are composed of Sn and O. The double peaks located at the binding energy of 486.7 and 495.2 eV with a spin–orbit splitting energy of 8.5 eV can be ascribed to the Sn $3d_{5/2}$ and Sn $3d_{3/2}$, respectively. As shown in Fig. 7, except for SnO_2 , the Sn $3d_{5/2}$ peak can be

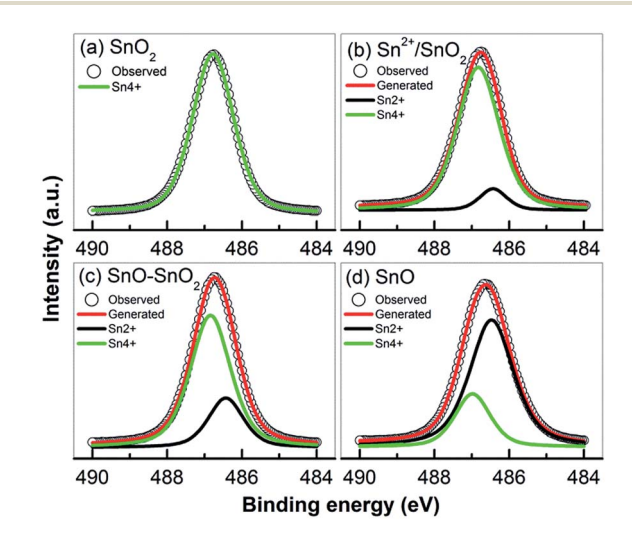


Fig. 7 High resolution XPS of Sn $3d_{5/2}$ peak taken form (a) SnO₂, (b) Sn²⁺-SnO₂ (prepared at 160 °C), (c) SnO/SnO₂ (prepared in 3 g urea added solution), and (d) SnO.

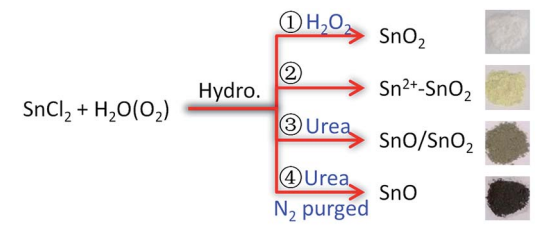
Paper **RSC Advances**

deconvoluted into two peaks centered at 486.4 and 486.8 eV, which can be assigned to Sn²⁺ and Sn⁴⁺, respectively.⁵⁵ The lack of a prominent binding energy shift of Sn 3d for different oxidation states can be attributed to the Madelung effects.⁵⁶ No Sn²⁺ signal can be detected in SnO₂ (Fig. 7a) suggesting that the oxidation of Sn²⁺ to Sn⁴⁺ can be effectively achieved by adding H₂O₂ into the solution. However, as shown in Fig. 7b, if no H₂O₂ was added, although most of Sn2+ was oxidized to Sn4+ by the dissolved O₂, about 9.3% Sn²⁺ (based on the ratio of the Sn²⁺ and Sn4+ peak areas) was reserved due to the depletion of dissolved O₂. This Sn²⁺ can be incorporated into SnO₂ lattice as a self-doping element. When urea was added, the Sn²⁺ content was substantially improved to ca. 25.1%. The decomposition of urea at 160 °C provides an anaerobic environment to preserve more Sn²⁺ component, which is survived in a form of SnO as indicated by the XRD results (Fig. 4a). The signal of Sn⁴⁺ still can be found on the prepared SnO in Fig. 7d and its percentage is determined to be ca. 24.8%. Considering that XPS is a surface characterization technique and only trace amount of SnO2 was observed in the XRD pattern (Fig. 4a), this SnO₂ should be on SnO surface and is formed by the oxidation of Sn2+ in an ambient environment. 55,57 The bulk of the sample should still be SnO. Fig. S2-b† shows the high resolution of O 1s spectrum. All the samples exhibit a broad and asymmetric O 1s peak which can be resolved into two peaks, one centered at 530.0 eV and the other at 531.7 eV. The peaks can be assigned to the crystal lattice oxygen in SnO or SnO₂ (ref. 47) and the adsorbed O₂ or surface -OH group.38

The above results indicate that the composition of the product is determined by the atmosphere of the hydrothermal solution, which is achieved by controlling the solution composition. Sn²⁺ can be oxidized to Sn⁴⁺ along with its hydrolysis in H₂O. The dissolved O₂ serves as the oxidant. 11,41 Due to the limitation of O₂ content, some Sn²⁺ can survive as a self-doping monomer in the product, leading to the formation of Sn²⁺-SnO₂. This Sn²⁺ residue can be eliminated by adding H₂O₂ into the solution. Then pristine SnO2 can be produced. But when urea was added, the decomposition of urea at 160 °C (ref. 58) could lead to a mixture atmosphere of O2 and CO2. Some part of Sn²⁺ precursor then was oxidized to SnO₂, while the other was converted to SnO under the protection of CO2, resulting in a SnO/SnO2 composite. In this urea-contained solution, if the dissolved O2 was removed by purging with N2 before the hydrothermal treatment, SnO then can be produced. The traces of SnO2 in SnO as shown in Fig. 4 may be caused by the oxidization of SnO, which occurs during the collection or storage of SnO. The selective preparation of these Sn oxides is briefly described in Scheme 1.

Photocatalytic activity

The visible light photocatalytic performances of the prepared samples were examined by the degradation of MO. Fig. S3 and S4† show the time-dependent decolorization of MO over the prepared samples. As shown in Fig. S5,† the azo bond (N=N) and the two benzene rings in MO give for the maximum absorption band at 465 nm (B1) and the small one at 270 nm



- (1) $Sn^{2+} + OH^{-} + H_2O_2 \rightarrow Sn(OH)_4 \rightarrow SnO_2$
- ② $Sn^{2+} + OH^{-} + O_{2} \rightarrow Sn(OH)_{x (2 < x < 4)} \rightarrow Sn^{2+} SnO_{2}$
- $CO(NH_2)_2 + H_2O \rightarrow NH_4^+ + CO_2 + OH^ \operatorname{Sn}^{2+} + \operatorname{OH}^- + \operatorname{O}_2 + \operatorname{CO}_2 \rightarrow \operatorname{Sn}(\operatorname{OH})_2 + \operatorname{Sn}(\operatorname{OH})_4 \rightarrow \operatorname{SnO/SnO}_2$
- 4 Sn²⁺ + OH⁻ + N₂ \rightarrow Sn(OH)₂ \rightarrow SnO

Scheme 1 Briefly diagram the conversion of SnCl₂ to the desired Sn oxides by controlling the hydrothermal solution composition.

(B2), respectively. 59 In the presence of Sn2+-SnO2 and SnO/SnO2, a decrease of B1 with irradiation time can be observed in Fig. S3 and S4,† suggesting the destruction of the conjugated structure of MO. After irradiation for ca. 60 min, a complete decolorization of MO can be realized over these samples except for Sn²⁺-SnO₂ prepared at 200 °C (Fig. S3-e†) and the solutions become colourless (as shown in the inset of Fig. S4-d†). However, the absorption of B2 still can be observed and is even improved with irradiation time. The increase of B2 suggests that these samples have low activity to cleave the highly stable aromatic rings. The accumulation of the fragments formed from the destruction of the chromophore bond accounts for the increase of B2. MO cannot be decolorized by the prepared SnO2 (Fig. S3-f†) as it cannot be activated by visible light. This result eliminates the possibility that the decolorization of MO is caused by a photosensitized oxidative process.60 Blank tests indicate that MO cannot be decomposed without the photocatalyst or the irradiation (Fig. S3-g and h†). Although SnO shows the highest visible light absorption coefficient, only 10% MO was decolorized after irradiation for 50 min. This may be caused by the fact that the 'OH which accounts for the decolorization of MO cannot be effectively produced on SnO (see below) and the BET surface area is as low as 5.2 m² g⁻¹ (Table 1).

The temporal change of MO concentration was measured by the absorbance of B1 to compare the photocatalytic performance of the prepared samples. As shown in Fig. 8, the activity of Sn²⁺-SnO₂ is slightly improved by enhancing the preparation temperature from 120 to 160 °C, then drops sharply with further increasing the temperature to 200 °C. Only 43% MO was decolorized after irradiation for 70 min on the sample prepared at 200 °C. The sample prepared at 160 °C shows the highest activity and the complete decolorization of MO can be achieved within 30 min. As the BET surface area of Sn²⁺-SnO₂ samples is around 100 m² g⁻¹ (Table 1), the activity reduction of the samples prepared at high temperature should be caused by the decrease of Sn²⁺ doping amount. As for the prepared SnO/SnO₂, the activity seems less impacted by the urea amount, as well as the BET surface area (ca. 78 m 2 g $^{-1}$, Table 1). Their activities are comparable to each other.

RSC Advances

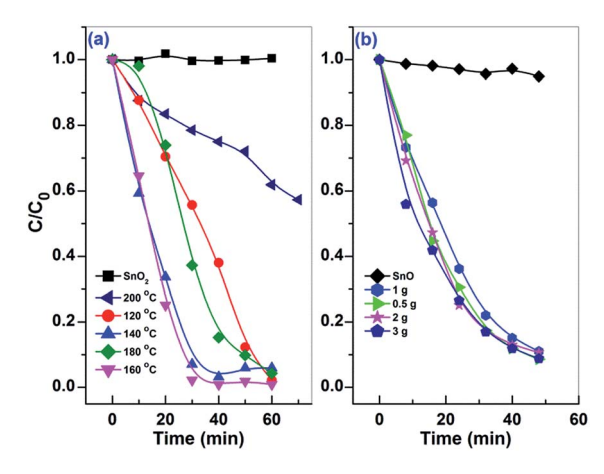


Fig. 8 The temporal changes of MO concentration with irradiation time over the (a) Sn²⁺-SnO₂ prepared at different temperatures and SnO₂, and (b) SnO/SnO₂ prepared in different urea-contained solutions and SnO.

The photocatalytic stability of Sn²⁺-SnO₂ and SnO/SnO₂ was investigated by reusing the photocatalysts. Unfortunately, as shown in Fig. 9, a deactivation of the samples can be observed. The activity can sustain for 3 runs on Sn²⁺-SnO₂, while on SnO/ SnO₂, it can only sustain for 1 run. Considering that the visible light photocatalytic activity is originated from Sn²⁺ species and the oxidation potential of Sn2+ to Sn4+ is only 0.15 V (vs. SHE),11,41 the deactivation of the samples is caused by the oxidation of Sn²⁺ to Sn⁴⁺ during the reaction.

3.4 Proposed reaction mechanism

The photocurrents of the prepared Sn²⁺-SnO₂, SnO/SnO₂, SnO, and SnO2 were measured under visible light irradiation to

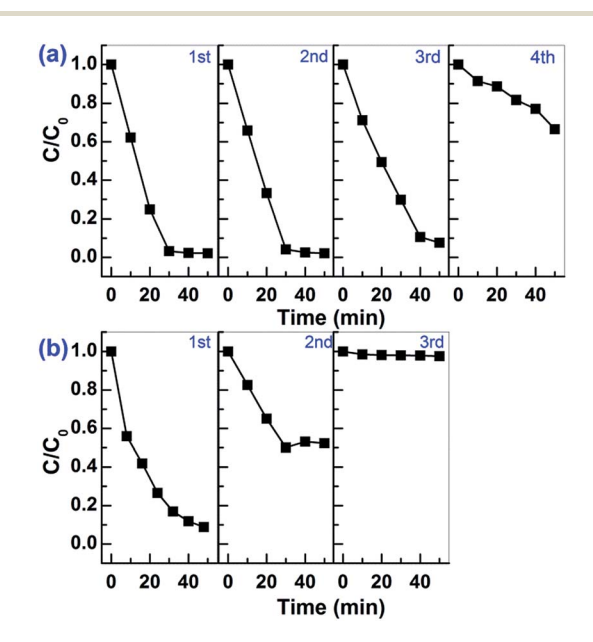


Fig. 9 Cycling tests for the photocatalytic decolorization of MO on (a) Sn²⁺-SnO₂ prepared at 160 °C and (b) SnO-SnO₂ prepared in 3 g urea added solution.

investigate the generation and the separation of the photoinduced charge carriers. As shown in Fig. 10, only Sn²⁺-SnO₂ and SnO/SnO₂ show apparent reversible photocurrent responses with light on and off. The result confirms that a visible light response can be involved by doping SnO₂ with Sn²⁺ or coupling it with SnO. Surprisingly, although SnO/SnO₂ shows a comparable photocatalytic activity to Sn²⁺-SnO₂, the photocurrent density of SnO/SnO₂ is substantially lower than the latter. A decay of the photocurrent with irradiation time can be observed on both of the samples, further suggesting their instability. Although SnO shows a visible light absorption, the photocurrent is negligible. It seems that the photo-induced charge carriers are consumed by SnO itself, rather than migrating to the surface to form a current. This may be the reason why SnO shows quite low performance for the decolorization of MO (Fig. 8b) and the activity of SnO/SnO2 can only sustain for one run (Fig. 9b). The photocurrent of SnO2 is negligible as it cannot be activated under visible light.

The photocurrent results suggest that the charge carriers can be generated on Sn²⁺-SnO₂ and SnO/SnO₂ under visible light irradiation. These charge carriers can further react with the adsorbed -OH, H2O, and O2 to form the active radicals. 'OH is one of the key active species for the degradation of pollutants. According to the band structures of SnO/SnO₂ and Sn²⁺-SnO₂ (Fig. S6†), 'OH can be induced by the photogenerated h⁺ in these samples as the standard reduction potential of 'OH/-OH is 1.99 V. 'OH formed on these samples was trapped by TA. As shown in Fig. S7,† the characterized fluorescence peak of TAOH at 425 nm can be observed on the prepared Sn²⁺-SnO₂ (Fig. S7ae†) and SnO/SnO₂ (Fig. S7g-k†) and the signal increases gradually with irradiation time. It suggests that the prepared Sn²⁺ incorporated SnO2 samples have the capability to form 'OH under the visible light irradiation. For SnO, the formation of TAOH is far slower than the Sn²⁺ incorporated SnO₂ samples and ceased after irradiation for ca. 25 min. Other control tests indicated that the formation of 'OH on SnO2 is negligible and cannot be perceived for the tests without a photocatalyst or illumination (Fig. S7m-o†). The formation efficiency of 'OH on

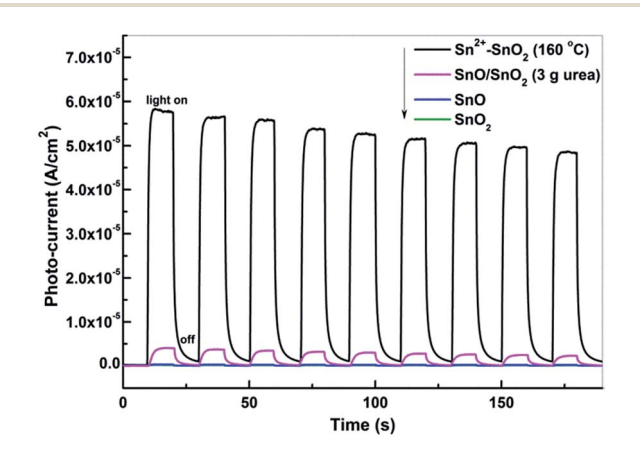


Fig. 10 Photocurrent responses of Sn²⁺-SnO₂ prepared at 160 °C, SnO/SnO₂ prepared in 3 g urea added solution, SnO, and SnO₂ under visible light irradiation ($\lambda > 400$ nm).

the prepared Sn²⁺-SnO₂ and SnO/SnO₂ samples is generally in agreement with their photocatalytic performances shown in Fig. 8. This relevance suggests that at least 'OH accounts for the degradation of MO. The visible-light-induced e⁻ and h⁺ are aroused by the doping of Sn²⁺ (ref. 41) or the coupling of SnO component^{38,40,61} (the electronic contributions from 5s orbitals of Sn²⁺). These charge carriers can be trapped by O₂, H₂O, or adsorbed -OH to generate 'OH or other oxidative species, which

eventually lead to the decomposition of MO. Besides, Sn²⁺ also

can be oxidized to Sn⁴⁺ by these oxidative species, leading to the

deactivation of Sn2+-SnO2 and SnO/SnO2 (Fig. 9).

4. Conclusions

Paper

We have developed a simple and effective hydrothermal method to selective preparation of SnO₂, Sn²⁺-SnO₂, SnO/SnO₂, and SnO with SnCl2 as precursor. Through adding H2O2 or urea, the solution can be tuned from an O2-rich to O2 deficient atmosphere, which facilitates the transformation of Sn2+ to SnO2 and the preservation of Sn2+ (in a form of doping Sn2+ or SnO component), respectively. The absorption of SnO2 can be successfully extended to the visible light region after self-doping with Sn²⁺ or coupling with SnO, which endows a visible light photocatalytic activity for MO degradation. Unfortunately, due to the oxidation of Sn²⁺ to Sn⁴⁺, the activities of the samples are quite unstable. Further work is still required to improve their photo-stability. Nonetheless, we believe that this work provides a simple method to selective preparation of different Sn-based oxides, which is essential for their applications, such as the detection of NO and NO2 based on SnO or SnO2.61 The work also provides a useful concept that is, through controlling the atmosphere of the solution, the oxidation state of metal oxides can be readily tuned by a hydrothermal method.

Acknowledgements

This work was financially supported by National Natural Science Foundation of China (Grant No. 21473066, 21603002, and 51472005), Natural Science Foundation of Anhui Province (Grant No. 1608085QB37).

Notes and references

- 1 W. Xia, H. Wang, X. Zeng, J. Han, J. Zhu, M. Zhou and S. Wu, *CrystEngComm*, 2014, **16**, 6841–6847.
- 2 E. Comini, Anal. Chim. Acta, 2006, 568, 28-40.
- 3 H. B. Wu, J. S. Chen, H. H. Hng and X. W. Lou, *Nanoscale*, 2012, 4, 2526–2542.
- 4 K. Ellmer, Nat. Photonics, 2012, 6, 809-817.
- 5 J. S. Chen and X. W. Lou, *Small*, 2013, **9**, 1877–1893.
- 6 M. Batzill and U. Diebold, Prog. Surf. Sci., 2005, 79, 47-154.
- 7 Y. Idota, T. Kubota, A. Matsufuji, Y. Maekawa and T. Miyasaka, *Science*, 1997, **276**, 1395–1397.
- 8 H. Wang and A. L. Rogach, Chem. Mater., 2014, 26, 123-133.
- 9 Z. Han, N. Guo, F. Li, W. Zhang, H. Zhao and Y. Qian, *Mater. Lett.*, 2001, 48, 99–103.

- 10 S. Mathur, R. Ganesan, I. Grobelsek, H. Shen, T. Ruegamer and S. Barth, *Adv. Eng. Mater.*, 2007, **9**, 658–663.
- 11 H. Wang, K. Dou, W. Y. Teoh, Y. Zhan, T. F. Hung, F. Zhang, J. Xu, R. Zhang and A. L. Rogach, *Adv. Funct. Mater.*, 2013, 4847–4853, DOI: 10.1002/adfm.201300303.
- 12 Z. Li, Y. Zhou, T. Yu, J. Liu and Z. Zou, *CrystEngComm*, 2012, 14, 6462–6468.
- 13 A. Kar, S. Sain, S. Kundu, A. Bhattacharyya, S. Kumar Pradhan and A. Patra, *ChemPhysChem*, 2015, **16**, 1017–1025.
- 14 A. K. Sinha, M. Pradhan, S. Sarkar and T. Pal, *Environ. Sci. Technol.*, 2013, 47, 2339–2345.
- 15 Z. D. Li, Y. Zhou, J. C. Song, T. Yu, J. G. Liu and Z. G. Zou, *J. Mater. Chem. A*, 2013, 1, 524–531.
- 16 D. Chu, J. Mo, Q. Peng, Y. Zhang, Y. Wei, Z. Zhuang and Y. Li, Chemcatchem, 2011, 3, 371–377.
- 17 M. Wang, Y. Gao, L. Dai, C. Cao and X. Guo, J. Solid State Chem., 2012, 189, 49–56.
- 18 S. Wu, H. Cao, S. Yin, X. Liu and X. Zhang, J. Phys. Chem. C, 2009, 113, 17893–17898.
- 19 H. Chen, C. E. Nanayakkara and V. H. Grassian, *Chem. Rev.*, 2012, **112**, 5919–5948.
- 20 M. R. Hoffmann, S. T. Martin, W. Y. Choi and D. W. Bahnemann, *Chem. Rev.*, 1995, 95, 69–96.
- 21 Y. C. Zhang, L. Yao, G. S. Zhang, D. D. Dionysiou, J. Li and X. H. Du, *Appl. Catal.*, B, 2014, 144, 730–738.
- 22 Y. C. Zhang, Z. N. Du, K. W. Li, M. Zhang and D. D. Dionysiou, ACS Appl. Mater. Interfaces, 2011, 3, 1528–1537.
- 23 Y. Zhao, Y. Zhang, J. Li and Y. Chen, Sep. Purif. Technol., 2014, 129, 90–95.
- 24 K. Vinodgopal and P. V. Kamat, *Environ. Sci. Technol.*, 1995, **29**, 841–845.
- 25 N. Chadwick, S. Sathasivam, A. Kafizas, S. M. Bawaked, A. Y. Obaid, S. Al-Thabaiti, S. N. Basahel, I. P. Parkin and C. J. Carmalt, *J. Mater. Chem. A*, 2014, 2, 5108–5116.
- 26 L. Zheng, Y. Zheng, C. Chen, Y. Zhan, X. Lin, Q. Zheng, K. Wei and J. Zhu, *Inorg. Chem.*, 2009, 48, 1819–1825.
- 27 W. Cun, X. M. Wang, B. Q. Xu, J. C. Zhao, B. X. Mai, P. Peng, G. Y. Sheng and H. M. Fu, *J. Photochem. Photobiol.*, A, 2004, 168, 47–52.
- 28 J. Wang, H. Li, S. Meng, L. Zhang, X. Fu and S. Chen, *Appl. Catal.*, *B*, 2017, **200**, 19–30.
- 29 H. Ullah, A. Khatoon and Z. Akhtar, *Mater. Res. Express*, 2014, 1, 045001.
- 30 D. Qi, L. Lu, Z. Xi, L. Wang and J. Zhang, *Appl. Catal.*, *B*, 2014, **160–161**, 621–628.
- 31 I. S. Chae, M. Koyano, K. Oyaizu and H. Nishide, *J. Mater. Chem. A*, 2013, **1**, 1326–1333.
- 32 A. Wahl and J. Augustynski, *J. Phys. Chem. B*, 1998, **102**, 7820–7828.
- 33 J. Jiang, L. Z. Zhang, H. Li, W. W. He and J. J. Yin, *Nanoscale*, 2013, 5, 10573–10581.
- 34 Y. Hosogi, Y. Shimodaira, H. Kato, H. Kobayashi and A. Kudo, *Chem. Mater.*, 2008, **20**, 1299–1307.
- 35 A. Naldoni, M. Allieta, S. Santangelo, M. Marelli, F. Fabbri, S. Cappelli, C. L. Bianchi, R. Psaro and V. Dal Santo, *J. Am. Chem. Soc.*, 2012, **134**, 7600–7603.

- 36 T. Xia and X. B. Chen, J. Mater. Chem. A, 2013, 1, 2983-2989.
- 37 A. Iwaszuk and M. Nolan, *J. Mater. Chem. A*, 2013, **1**, 6670–6677.
- 38 A. K. Sinha, P. K. Manna, M. Pradhan, C. Mondal, S. M. Yusuf and T. Pal, *RSC Adv.*, 2014, 4, 208–211.
- 39 K. Santhi, C. Rani and S. Karuppuchamy, *J. Alloys Compd.*, 2016, 662, 102–107.
- 40 A. Roy, S. Arbuj, Y. Waghadkar, M. Shinde, G. Umarji, S. Rane, K. Patil, S. Gosavi and R. Chauhan, *J. Solid State Electrochem.*, 2016, 1–9, DOI: 10.1007/s10008-016-3328-y.
- 41 C. M. Fan, Y. Peng, Q. Zhu, L. Lin, R. X. Wang and A. W. Xu, *J. Phys. Chem. C*, 2013, **117**, 24157–24166.
- 42 Y. He, D. Li, J. Chen, Y. Shao, J. Xian, X. Zheng and P. Wang, *RSC Adv.*, 2014, **4**, 1266–1269.
- 43 Q. Yan, J. Wang, X. Han and Z. Liu, *J. Mater. Res.*, 2013, 28, 1862–1869.
- 44 G. Chen, S. Ji, Y. Sang, S. Chang, Y. Wang, P. Hao, J. Claverie, H. Liu and G. Yu, *Nanoscale*, 2015, 7, 3117–3125.
- 45 H. Uchiyama, H. Ohgi and H. Imai, *Cryst. Growth Des.*, 2006, **6**, 2186–2190.
- 46 J. R. Sambrano, L. A. Vasconcellos, J. B. L. Martins, M. R. C. Santos, E. Longo and A. Beltran, *J. Mol. Struct.:* THEOCHEM, 2003, 629, 307–314.
- 47 J. Mazloom, F. E. Ghodsi and H. Golmojdeh, *J. Alloys Compd.*, 2015, **639**, 393–399.
- 48 X. Fu, D. Y. C. Leung and S. Chen, *CrystEngComm*, 2014, **16**, 616–626.

- 49 J. Tauc, R. Grigorovici and A. Vancu, *Phys. Status Solidi*, 1966, 15, 627–637.
- 50 T. Arai and S. Adachi, ECS J. Solid State Sci. Technol., 2012, 1, R15–R21.
- 51 Z. Khodami and A. Nezamzadeh-Ejhieh, J. Mol. Catal. A: Chem., 2015, 409, 59–68.
- 52 H. Chen, L. Ding, W. Sun, Q. Jiang, J. Hu and J. Li, RSC Adv., 2015, 5, 56401–56409.
- 53 L. Zhang, H. Zhang, H. Huang, Y. Liu and Z. Kang, *New J. Chem.*, 2012, **36**, 1541–1544.
- 54 G. Sun, N. Wu, Y. Li, J. Cao, F. Qi, H. Bala and Z. Zhang, *Mater. Lett.*, 2013, **98**, 234–237.
- 55 G. Zhou, X. Wu, L. Liu, X. Zhu, X. Zhu, Y. Hao and P. K. Chu, *Appl. Surf. Sci.*, 2015, **349**, 798–804.
- 56 V. B. R. Boppana and R. F. Lobo, *J. Catal.*, 2011, **281**, 156–168.
- 57 H.-R. Kim, K.-I. Choi, J.-H. Lee and S. A. Akbar, *Sens. Actuators*, *B*, 2009, **136**, 138–143.
- 58 W. K. Choi, H. Sung, K. H. Kim, J. S. Cho, S. C. Choi, H. J. Jung, S. K. Koh, C. M. Lee and K. Jeong, *J. Mater. Sci. Lett.*, 1997, 16, 1551–1554.
- 59 T. Tasaki, T. Wada, K. Fujimoto, S. Kai, K. Ohe, T. Oshima, Y. Baba and M. Kukizaki, J. Hazard. Mater., 2009, 162, 1103–1110.
- 60 T. X. Wu, G. M. Liu, J. C. Zhao, H. Hidaka and N. Serpone, *J. Phys. Chem. B*, 1998, **102**, 5845–5851.
- 61 L. Li, C. Zhang and W. Chen, *Nanoscale*, 2015, 7, 12133–12142.